

Uncertainty Structure and μ -Synthesis of a Magnetic Suspension System

Member Toru Namerikawa (Kanazawa University)

Member Masayuki Fujita (Kanazawa University)

This paper deals with modeling, uncertain structure and μ -synthesis of a magnetic suspension system. The dynamics of magnetic suspension systems are characterized by their instability and complexity of electromagnets, and they should be robustly stabilized in spite of model uncertainties. First we derive a nominal design model of the plant under some assumption, then we investigate the gap between the real physical system and the obtained nominal design model. This gap has complex structure which is expressed by the structured uncertainties that includes linearization error, parametric uncertainties, and neglected dynamics. Then we set the interconnection structure which contains the above structurally represented uncertainties. Next we design a robust controller which achieves robust performance using the structured singular value μ . Finally, we evaluate the proposed interconnection structure and verify robustness and performance of the designed μ controller by several experiments.

Keywords: Magnetic Suspension Systems, Uncertain Model, Linear Fractional Transformation, Robust Control, μ -Analysis and Synthesis

1. Introduction

Active magnetic suspension systems allow contact-free suspension. They do not suffer from friction nor wear, and this is the most important advantage of these systems. This technology is now used for various industrial purposes, and has already been applied to magnetically levitated vehicles, magnetic bearings, etc.⁽¹⁾⁽²⁾. Recent overviews, advances and applications in this field can be seen in⁽³⁾⁻⁽⁵⁾.

Since an active controlled-type magnetic suspension system is inherently unstable, feedback control is indispensable to stabilize the system. A conventional PID controller is often employed as a feedback compensator, and this method often yields enough stability and performance, but owing to model uncertainties and changes of the operating points, the entire system sometimes becomes unstable.

To avoid this problem, the approach taken here is an application of robust control methodologies. It is well known this is one of the effective control techniques for unstable systems. On the control of magnetic suspension technology field, one of the most critical problems is a description of a complex behavior of the dynamics of electromagnets and their forces.

The exact description of this behavior is almost hopeless, and even if it should be achieved by infinite dimensional nonlinear differential equations, the resulting model is only effective for the simulations/analysis, but can not be used for a control system design as it is. Then some approximations and assumptions must be employed, and consequently the gaps between the real physical system and the design model cannot be

avoided.

There are so many results of robust control of magnetic suspension systems, but in these results, the above uncertainties have been treated as exogenous disturbances and as unstructured uncertainties⁽⁶⁾⁻⁽⁸⁾, however, both of the uncertainty descriptions lead to conservative analytic results for robust stability/performance tests. The goal of robust control theory is not only to get robust controllers but also to know the quantitative limitation of stability/performance of the controller.

In⁽⁹⁾⁻⁽¹¹⁾, parameter perturbations were considered, and the model uncertainties were described structurally, this result succeeded to reduce the conservativeness of analysis. But the considered model perturbation is imaginary and they assumed that all model parameters have same several percent uncertainties, but this assumption can not fit the real physical phenomenon.

Recently the state-space control theory of uncertain system with Linear Fractional Transformation(LFT) has almost been settled up for practical use⁽¹²⁾. LFT have come to play an important role in control system design, and provide a uniform framework for realization, analysis and synthesis for uncertain systems. Now its practical evaluation is extremely expected.

In this paper, we present the model and uncertainty description of a magnetic suspension system by using LFT, which contains less conservativeness for robust stability/performance analysis. Further we propose a method to quantify the magnitude of uncertainties.

Uncertainties we consider in this paper are the linearization error of the electromagnetic force, unmodeled dynamics of electromagnet, and parametric uncertainties. We structurally describe these three types

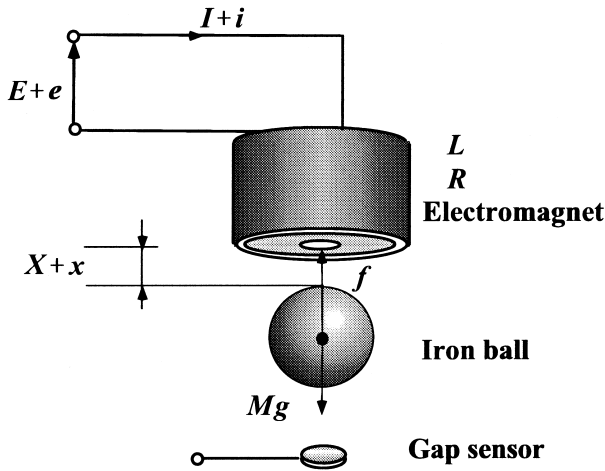


Fig. 1. Magnetic Suspension System

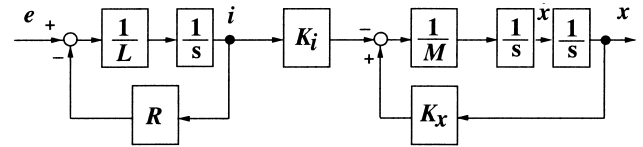


Fig. 2. Nominal linear model for M.S.S.

of uncertainties by using real/ complex bounded numbers/matrices. For robustness analysis, we employ the mixed structured singular value(mixed μ) test⁽¹³⁾ to reduce conservativeness.

Finally, based on an uncertainty model, we derived a μ controller. At the end of our paper, we evaluate the proposed model and uncertainty structure by several experimental results concerned to the robust stability and robust performance.

2. Magnetic Suspension System and its Model

In this section, we introduce the most basic magnetic suspension system which has only one degree of freedom. Then we derive an ideal mathematical model of the system based on physical laws and several assumptions.

2.1 Construction of the system Consider the electromagnetic suspension system shown schematically in Fig.1. An electromagnet is located at the top of the experimental system.

The control problem is to levitate the iron ball stably utilizing the electromagnetic force. The ball's mass M is 1.04kg, and steady state gap X is 5mm. Note that this simple electromagnetic suspension system is unstable without feedback control. A standard induction probe of eddy current type gap sensor is placed below the ball to detect the distance between the iron ball and the electromagnet.

2.2 Mathematical Model First, we introduce following assumptions⁽¹⁾⁽²⁾⁽⁶⁾ in order to derive a nominal model of this system by physical laws.

- [A1] Magnetic flux density and magnetic field do not have any hysteresis, and they are not saturated.
- [A2] There is no leakage of flux in the magnetic circuit.
- [A3] Magnetic permeability of the electromagnet is infinite.
- [A4] Eddy currents in the magnetic pole can be neglected.
- [A5] Coil inductance is constant around the operating point, and any electromotive force due to a motion of the iron ball can be neglected.

These assumptions are not very strong and suitable around the steady state.

Under these assumptions, we derive the following three equations, which show an equation of the motion of the iron ball, electromagnetic force and equation of an electric circuit of the electromagnet, respectively.

$$M \frac{d^2 x(t)}{dt^2} = Mg - f(t), \dots\dots\dots (1)$$

$$f(t) = k \left(\frac{I + i(t)}{X + x(t) + x_0} \right)^2, \dots\dots\dots (2)$$

$$L \frac{di(t)}{dt} + R(I + i(t)) = E + e(t), \dots\dots\dots (3)$$

where M is the mass of the iron ball, X is the steady gap between the electromagnet(EM) and the iron ball, $x(t)$ is the deviation from X , I is the steady current, $i(t)$ is the deviation from I , E is the steady voltage, $e(t)$ is the deviation from E , $f(t)$ is the electromagnetic force, k and x_0 are coefficients of $f(t)$ which are determined by experiments, L is an inductance of the EM, and R is a resistance of the EM.

In the case we apply the linear control theory with respect to this system, the problem is that the equation of the electromagnetic force (2) is nonlinear concerning $x(t)$ and $i(t)$. Here we utilize the standard linearization approach based on the Taylor series expansion around the operating point.

$$f(t) := k \left(\frac{I}{X + x_0} \right)^2 - K_x x(t) + K_i i(t),$$

$$K_x := \frac{2kI^2}{(X + x_0)^3}, \quad K_i := \frac{2kI}{(X + x_0)^2}. \dots\dots (4)$$

Moreover, the steady state equations are given by $Mg = k \left(\frac{I}{X+x_0} \right)^2$ and $RI = E$, then according to equations (1), (3), (4) and these two steady state equations, the nominal transfer function of the magnetic suspension system is easily derived as

$$G_{nom}(s) := \frac{-K_i}{(Ms^2 - K_x)(Ls + R)}. \dots\dots\dots (5)$$

This equation shows the system is unstable and oscillatory. Further, in Fig.2 the nominal block diagram of the magnetic suspension system is shown, and it shows the structure of the plant. The positive feedback from x to \ddot{x} through K_x makes the system unstable.

The nominal model parameters are given in Table 1.

Table 1. Model Parameters

Parameter	Nominal Value	Unit
M	1.04	[kg]
X	5.00×10^{-3}	[m]
I	0.789	[A]
k	1.71×10^{-4}	$[Nm^2/A^2]$
x_0	-1.80×10^{-3}	[m]
K_x	6.27×10^3	$[N/m]$
K_i	25.7	$[N/A]$
L	0.859	[H]
R	24.76	$[\Omega]$

3. Structured Uncertainties

The derived nominal model (5) and/or Fig. 2 with nominal model parameters works fairly well around the steady state operational point. However, if the state of the system deviates from the nominal operating point, the model no longer suitably describes the physical system.

We treat this gap as a model uncertainty, and we make a new extended model, which is a set of plant models, that is constructed with the nominal model and model uncertainties. This set of models can cover the relatively wider behaviors of the real plant, but still not globally. This set is an extension of the nominal model. The following three items are well known to be the most general and serious uncertainties⁽¹⁴⁾:

- Linearization Error
- Parametric Uncertainty
- Unmodeled Dynamics

We discuss these uncertainties in the following sections, and include them into the set.

3.1 Linearization Error There should be model uncertainties caused by linearization of the electromagnetic force, which was generated by the approximation from equation (2) to (4).

In Fig.3, Current-Force ($i - f$) curve for a gap width $X=5.0\text{mm}$ is plotted in the upper figure, and Gap-Force ($x - f$) curve at current $I=1.15\text{A}$ is depicted in the lower figure, where a symbol “o” denotes measured experimental data at each point, and solid curved lines show the determined Current-Force and Gap-Force curve, respectively. These curves are determined from the least squares approximation laid on the equation (2). Two dashed straight lines indicate tangents of each curve at the operating points. These inclinations of tangents are employed as K_i and K_x from equation (4), respectively. The four dash-dot straight lines are sectors of the linearization errors, which we will use them as sector bounds in the following.

Fig.3 shows that the perturbations between tangents and curves become bigger if the operating points move from the original points. These errors were caused by linearization. Here we employ sector bounds to account for the linearization error, and describe K_i and K_x as

$$K_i := K_{i0} + k_i \delta_i, \quad |\delta_i| \leq 1, \dots\dots\dots (6)$$

$$K_x := K_{x0} + k_x \delta_x, \quad |\delta_x| \leq 1, \dots\dots\dots (7)$$

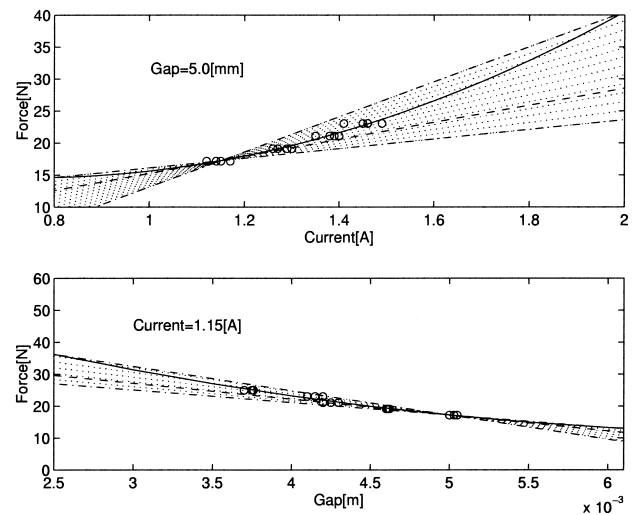


Fig. 3. Current-Force Curve and Gap-Force Curve

where K_{i0} and K_{x0} are nominal values, k_i and k_x are uncertainty weights determined from slopes of the dash-dotted lines.

3.2 Parametric Uncertainty The first request for the system is robust stability against unexpected exogenous force disturbances. Another general demand in practical use of the magnetic suspension system is a flexible change of the mass of suspended objects. These two specifications can be described by a parametric perturbation of a mass of the iron ball M . We describe it as

$$\frac{1}{M} = \frac{1}{M_0 + k_M \delta_M}, \quad |\delta_M| \leq 1, \dots\dots\dots (8)$$

where M_0 is the nominal value, and k_M is an uncertainty weight.

3.3 Unmodeled Dynamics In this section, we discuss the dynamics of electromagnets. Nominally it is expressed by a transfer function $G_{EM}(s) := \frac{1}{Ls + R}$. It is well known that an inductance L and a resistance R of the electromagnet have frequency varying and gap(x)-dependent characteristics. Further, these parameters are very sensitive to be measured. Nominal values of L and R are determined as averages of five measurements under the condition $f = 10\text{Hz}$ and $X = 5\text{mm}$. Figure 4 shows the experimental data of $G_{EM}(s)$, where the solid curved line indicates the nominal frequency response which is located in the center of a band, dashed lines show upper and lower bounds.

The transfer functions of the electromagnet are distributed in a frequency dependent belt. Furthermore, if the frequency of the input signal changes, this belt becomes broad. We describe this belt as an unstructured uncertainty of the following:

$$G_{EM}(s) := \frac{1}{L_0 s + R_0} + w_i(s) \Delta_i(s), \quad |\Delta_i(j\omega)| \leq 1. \dots\dots\dots (9)$$

Where L_0 and R_0 , are the nominal values of L and

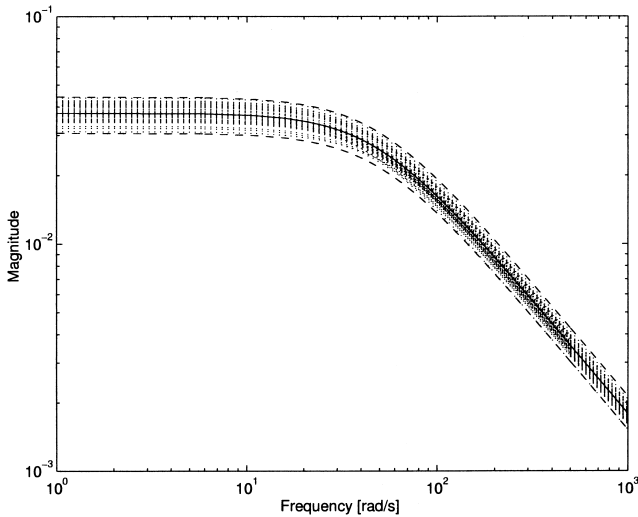


Fig. 4. Frequency responses of $G_{EM}(s)$

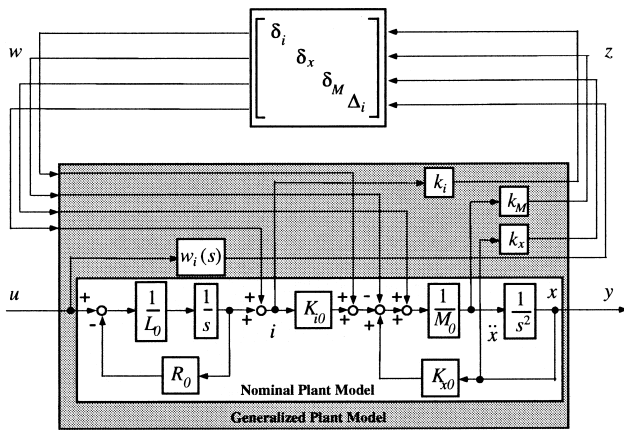


Fig. 5. Set of Plant Models with Uncertainties: $\tilde{G}(s)$

R , respectively, and $w_i(s)$ is an uncertainty weight. The magnitude of the weight $w_i(s)$ is determined as half of the width of the belt in Fig.4.

3.4 Set of Plant Models: $\tilde{G}(s)$ Up to now, three types of uncertainties have been considered. Now in this section, we use them to construct a model of this plant. Actually, we make a set of plant models $\tilde{G}(s)$ in LFT form⁽¹²⁾ which includes the above nominal model, linearization error, parametric uncertainties, and unmodeled dynamics. Using the LFT representation, then the block diagram model of the system is replaced from Fig.2 to Fig.5. The state space representation of $\tilde{G}(s)$ is easily derived, so in this paper it is omitted. Now we have extended the nominal model and obtained a set of plant models by LFT representation which is expected to express the relatively wider behaviors of the real plant.

4. μ -Analysis and Synthesis

In this section, we design a robust controller for the set of models $\tilde{G}(s)$

4.1 Quantification of Uncertainties The obtained set of models $\tilde{G}(s)$ gives only a structure of the uncertainties, not a quantity of each uncertainty.

In the previous research, tuning of the design parameters was depended on experimental/ simulated trial and error. Development of a systematic tuning method for the design parameters is now expected. Further, the physical limit of allowable perturbations for robust stability/performance was not clear. We quantify the amount of uncertainty based on a change of the operating point.

4.1.1 Change of the Operating Point Our approach taken here is to determine the set of the plant models based on the change of the operating point. The operating point of this system is characterized by a steady state gap $\{X \mid X_{\min} \leq X \leq X_{\max}\}$. As a design specification for real applications, the range $\{X \mid X_{\min} \leq X \leq X_{\max}\}$ is expected to be wider, but this change of the operating point X causes perturbations of K_i and K_x , hence the allowable range of the operating point $\{X \mid X_{\min} \leq X \leq X_{\max}\}$ is limited.

After the several iterations of controller design and control experiments, we have finally chosen the allowable range of the operation point as follows, where μ -synthesis based on $D - K$ iteration and the mixed μ -analysis were employed[13,15].

$$\{X \mid 3.8 \text{ mm} \leq X \leq 6.2 \text{ mm}\} \dots\dots\dots (10)$$

4.1.2 Perturbation of K_i and K_x Any change of the operating point X also causes the perturbations of the parameters K_i and K_x . We utilize Fig.3 to determine the bound of the perturbations of K_i and K_x . A magnetic force f and a gap X and a current I are related each other, and are written in (2). This equation (2) is transformed to (4) using the standard linearization approach based on the Taylor series expansion around the operating point.

The experimental data corresponding to (2) is Fig.3. A symbol “o” denotes measured experimental data at each point, and solid curved lines show the determined Current-Force and Gap-Force curve, respectively. These curves are determined from the least squares approximation laid on the equation (2). In Fig.3, Current-Force ($i - f$) curve for a gap width $X=5.0\text{mm}$ is plotted in the upper figure, and Gap-Force ($x - f$) curve at current $I=1.15\text{A}$ is depicted in the lower figure.

The following is a procedure to determine the bounds of perturbations of K_i and K_x .

- (1) First, decide the operating point X , which has a one-to-one correspondence to I , hence the I is fixed. The operating point in the horizontal axes in Figs 3 (upper and lower) have been fixed.
- (2) Calculate tangents of each curve at the operating points. These inclinations of tangents are employed as K_i and K_x from equation (4), respectively. In Fig. 3, two dashed straight lines indicate tangents.
- (3) Change the operating point, and continue step(1) and step(2).

In this case, parameters K_i and K_x perturb as $14.1 \leq K_i \leq 37.3$ and $5.38 \times 10^3 \leq K_x \leq 7.16 \times 10^3$ ($3.8 \leq X \leq 6.2$). Then we describe K_i and K_x as below.

$$K_i = 25.7 + 11.6 \cdot \delta_i, \quad |\delta_i| \leq 1, \dots\dots\dots (11)$$

$$K_x = 6.27 \times 10^3 + 8.90 \times 10^2 \cdot \delta_x, \\ |\delta_x| \leq 1. \dots\dots\dots (12)$$

4.1.3 Dynamical Uncertainties Uncertainties in the dynamics of electromagnet $w_i(s)$ is also considered in this section. $w_i(s)$ is not only an uncertainty of the dynamics of electromagnet but an important design parameter. After several design iterations, the final bound of $w_i(s)$ and $G_{EM}(s)$ has been chosen to obtain an appropriate robustness as below.

$$G_{EM}(s) := \frac{1}{0.859s + 24.8} \\ + \frac{1.28 \times 10^{-3}(s + 3.20)(s + 900)}{(s + 25.8)(s + 31.4)} \Delta_i(s), \\ |\Delta_i(j\omega)| \leq 1. \dots\dots\dots (13)$$

In this $w_i(s)$, the parametric uncertainty of L and R as $0.782 \leq L \leq 0.936$ (9% perturbation) and $24.5 \leq R \leq 25.0$ (1% perturbation) are involved. In addition to these parametric perturbation, unmodeled dynamics in the high frequency range is also included in $w_i(s)$. Frequency response of the final set of electromagnetic dynamics is shown in Fig. 6.

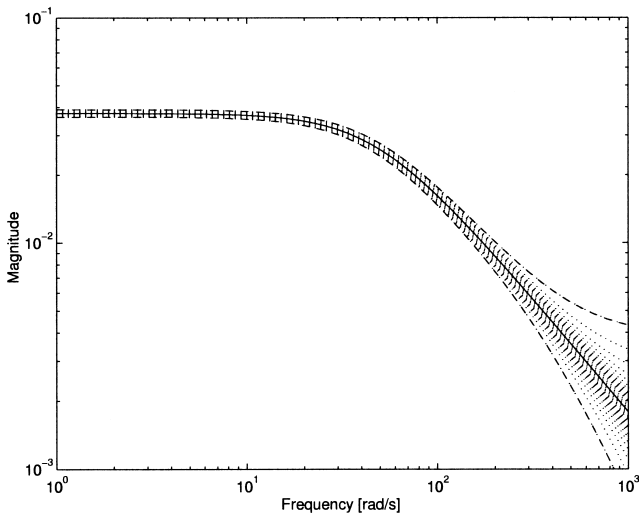


Fig. 6. Final transfer function $G_{EM}(s)$ with uncertainty $w_i(s)$

From the above discussion in these three subsections, the final quantity of uncertainties are selected in Table 2, where 7% perturbation of a mass M is considered. Final frequency response of $w_i(s)$ is shown in Fig.7.

4.2 Control System Design Utilizing the structured singular value $\mu^{(13)(15)(16)}$, we design the controller which achieves robust performance against various types of uncertainties.

Table 2. Quantity of uncertainties

	Value		Value
k_i	11.6	k_x	8.90×10^2
k_M	7.25×10^{-2}	$w_i(s)$	$\frac{1.28 \times 10^{-3}(s+3.20)(s+900)}{(s+25.8)(s+31.4)}$

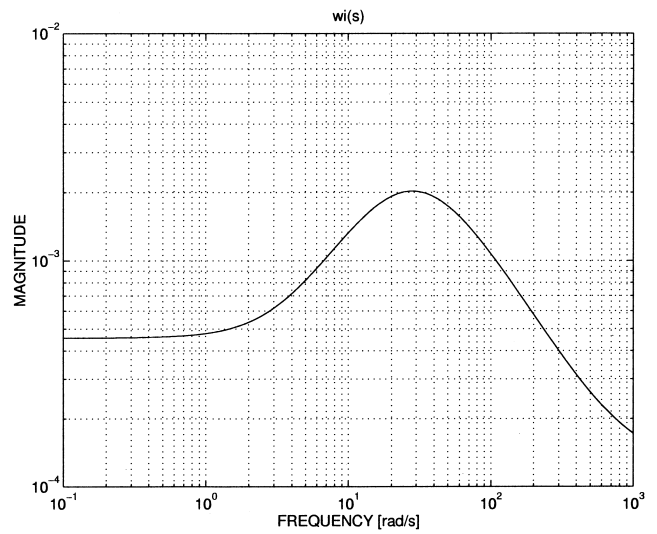


Fig. 7. Frequency response of the weight $w_i(s)$

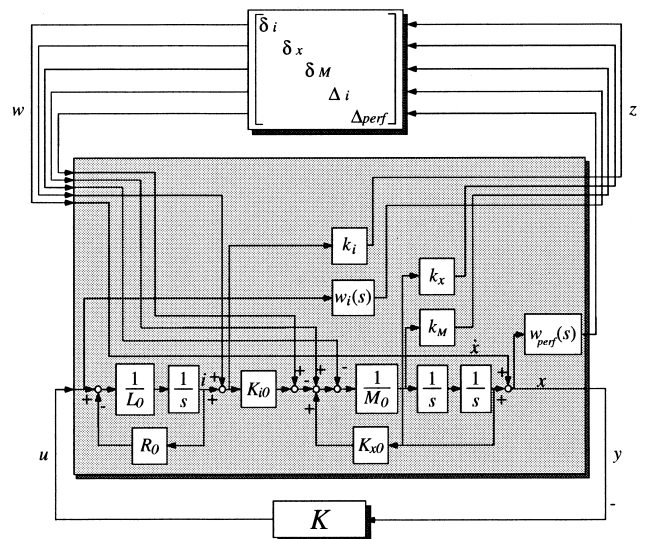


Fig. 8. Interconnection Structure

4.2.1 Interconnection structure We construct an interconnection structure by LFT representation in Fig.8, where W_{perf} is a performance specification and also is a weight for a sensitivity function $S := (I + G_{nom}K)^{-1}$.

For the disturbance attenuation and the tracking for reference signal, the controller is expected to have integral property. In order to achieve this specification, W_{perf} was chosen as the following function.

$$W_{perf}(s) = \frac{100}{1 + s/0.1}. \dots\dots\dots (14)$$

4.2.2 Control Problem Next, for the robust performance synthesis, we define the block structure Δ

as follows.

$$\Delta := \{\text{diag}[\delta_i, \delta_x, \delta_M, \Delta_i, \Delta_{perf}] : \delta_i, \delta_x, \delta_M \in \mathbf{R}, \Delta_i, \Delta_{perf} \in \mathbf{C}\} \dots \dots \dots (15)$$

It is well known that the structured singular value $\mu_{\Delta}(M)$ is defined for matrices $M \in \mathbf{C}^{n \times n}$ with the block structure Δ as

$$\mu_{\Delta}(M) := \frac{1}{\min\{\bar{\sigma}(\Delta) : \Delta \in \mathbf{\Delta}, \det(I - M\Delta) = 0\}} \quad (16)$$

unless no $\Delta \in \mathbf{\Delta}$ makes $(I - M\Delta)$ singular, in which case $\mu_{\Delta}(M) := 0$. Then, the control problem is to find the controller $K(s)$ which achieves the following robust performance condition, where $P(s)$ is the generalized plant which is expressed by the gray rectangle box in Fig.8.

$$\sup_{\omega \in \mathbf{R}} \mu_{\Delta}[F_l(P(j\omega), K(j\omega))(j\omega)] < 1. \dots \dots \dots (17)$$

We apply the standard $D - K$ iteration⁽¹⁶⁾ to find the sub-optimal μ controller for the system. We thus iteratively solve the following problem:

$$\sup_{\omega \in \mathbf{R}} \inf_{D(\omega)} \{\bar{\sigma}(D(j\omega)F_l(P, K)D^{-1}(j\omega))\} < 1. \quad (18)$$

The block structure (15) is used to calculate the mixed μ value (17), but the real-valued blocks in (15) are replaced to complex-valued ones in the calculating and fitting process of the scaling matrix D .

4.2.3 Robust μ Controller After the 3rd iteration, we obtained a controller $K(s)$, where the supremum of $\mu_{\Delta}[F_l(P, K)]$ is 0.9766. Final scaling matrix $D(s)$ has 12 states, then $K(s)$ has 30 states. We employed the Hankel norm approximation technique to calculate the reduced order system of $K(s)$. Final balanced controller $\hat{K}(s)$ is as follows, and its bode diagram is shown in Fig.9. The supremum of the $\mu_{\Delta}[F_l(P, \hat{K})]$ is also 0.9766.

$$\begin{aligned} \hat{K}(s) = & \frac{3.27 \times 10^{10} \times (s + 486 \pm 885i)}{(s + 1740)(s + 949 \pm 1320i)} \\ & \times \frac{(s + 389 \pm 626i)(s + 335)(s + 79.1)}{(s + 472 \pm 794i)(s + 391 \pm 599i)} \\ & \times \frac{(s + 29.5)(s + 14.7)(s + 4.86)}{(s + 348)(s + 8.16)(s + 2.66)} \\ & \times \frac{(s + 2.63)(s + 0.175)(s + 0.114)}{(s + 0.210)(s + 0.127)(s + 0.0778)} \quad (19) \end{aligned}$$

Calculated upper and lower bounds of $\mu_{\Delta}[F_l(P, \hat{K})]$ with the controller $\hat{K}(s)$ are shown in Fig.10, where the two solid lines respectively show upper and lower bounds of μ and the dashed line shows the maximum singular value of $(D(j\omega)F_l(P(j\omega), \hat{K}(j\omega))(j\omega)D^{-1}(j\omega))$. Since the peak value of the upper bound of μ is

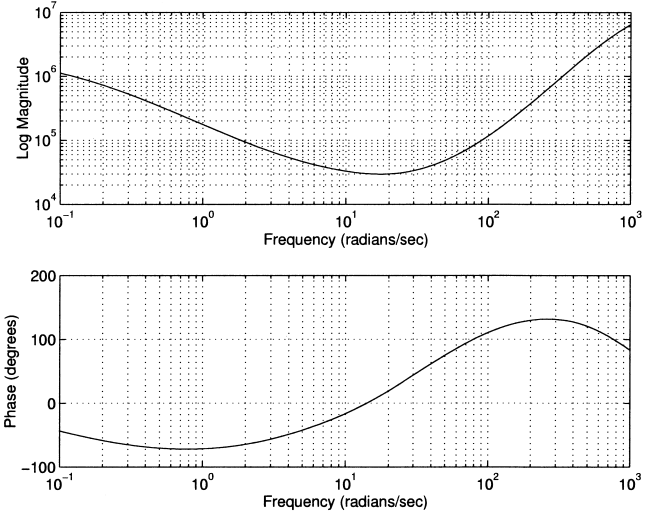


Fig. 9. Final Controller $\hat{K}(s)$

less than 1, the closed-loop system with uncertainties achieves the robust performance condition.

This result shows $\hat{K}(s)$ guarantees robust performance against uncertainties caused by a change of operating point $\{X \mid 3.8 \leq X \leq 6.2\}$ (10).

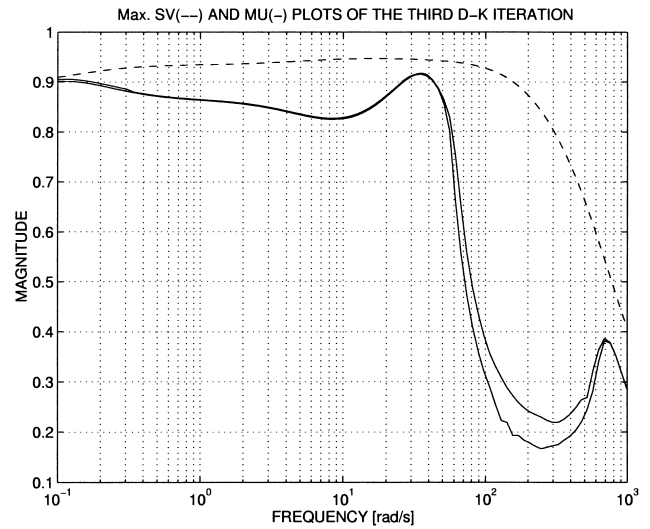


Fig. 10. $\mu_{\Delta}[F_l(P, \hat{K})]$ and $\bar{\sigma}[DF_l(P, \hat{K})D^{-1}]$

5. Experimental Evaluation

In order to evaluate the proposed set of plant models $\tilde{G}(s)$, we implement the obtained controller $\hat{K}(s)$ via a digital control system, and carried out experiments. The sampling period of the controller is 95 μ s, and a well known Tustin transform was employed for discretization. All experimental results of time response of the iron ball position are shown in Fig.11, 12, 13.

5.1 Evaluation of Nominal Performance Step response of the position x of the iron ball at $X = 5$ mm (nominal steady gap) is shown in Fig.11, which indicates the stable levitation with the controller $\hat{K}(s)$ at the nominal steady gap $X = 5.0$ mm. The magnitude

of the step-type disturbance is 22 N, which is twice as much as steady state force. Since it is difficult to give disturbance forces to the iron ball directly and repeatedly, we add pseudo-disturbance by applying voltage signal to the control input signal. This figure shows the nominal performance.

5.2 Evaluation of Robust Stability Next our interest is robust stability of the closed-loop system. Time responses of the controllers $\hat{K}(s)$ are shown in Fig.12, which indicate the stable levitation at the steady state gaps $X = 1.3, 5.0, 8.7$ mm.

- **The robust stability against the perturbation $\{ X \mid 1.3\text{mm} \leq X \leq 8.7\text{mm} \}$ is achieved.**

If we change the steady state gap X to less than $X = 1.3$, or greater than $X = 8.7$, however, the system disappointingly becomes unstable.

5.3 Evaluation of Robust Performance The final evaluative item is our main control problem, "robust performance". For the sake of verification of the robust performance, we measured time responses against a step-type external disturbance (22 N) at the steady state gaps $X = 3.8, 6.2$ mm. Results are shown in Fig.13. Apparently, the controller $\hat{K}(s)$ shows enough performance comparing the response in Fig11. We have confirmed that

- $\hat{K}(s)$ achieves the robust performance against model perturbations caused by a change of operating point $\{ X \mid 3.8\text{mm} \leq X \leq 6.2\text{mm} \}$ (10).

When we change the steady state gap X to $\{ X \mid 2.8\text{mm} \leq X \leq 7.2\text{mm} \}$, the system keep up the almost same response, but if the steady state gap X would be less than $X = 2.8$, or greater than $X = 7.2$, the response suddenly deteriorates.

6. Conclusion

In this paper, we proposed the novel model and uncertainty structure of magnetic suspension systems by using LFT, which contains less conservativeness for robust stability/performance analysis. Further we proposed one method to quantify the magnitude of uncertainties. Uncertainties we considered in this paper are the linearization error of the electromagnetic force, unmodeled dynamics of the electromagnet, and parametric uncertainties. We structurally described these three types of uncertainties by using real/ complex bounded numbers/matrices. Next, we designed a robust controller by μ -analysis and synthesis which achieves robust performance by using the structured singular value μ . Here, we employ the mixed μ test to reduce conservativeness.

Finally, we evaluate the proposed model and uncertainty structure by several experimental results concerned to the nominal performance, robust stability and robust performance.

Acknowledgment

The authors wish to thank Mr. Florian Lösch and Prof. Gerhard Schweitzer with ETH for helpful discussions and suggestions.

(Manuscript received July 3, 2000, revised December

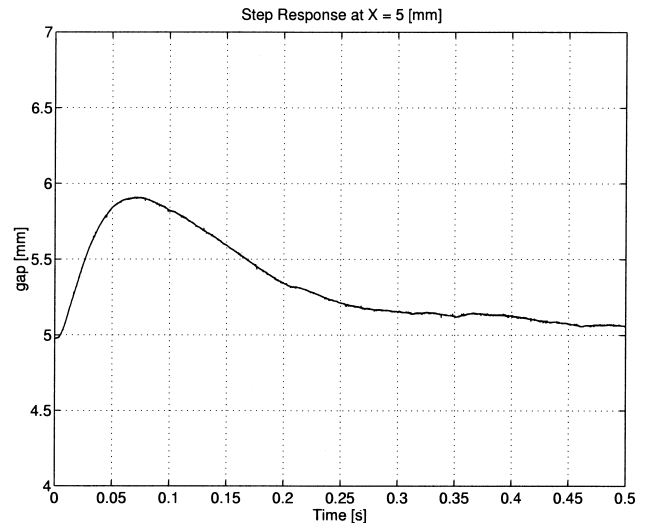


Fig. 11. Step Response at $X = 5$ mm

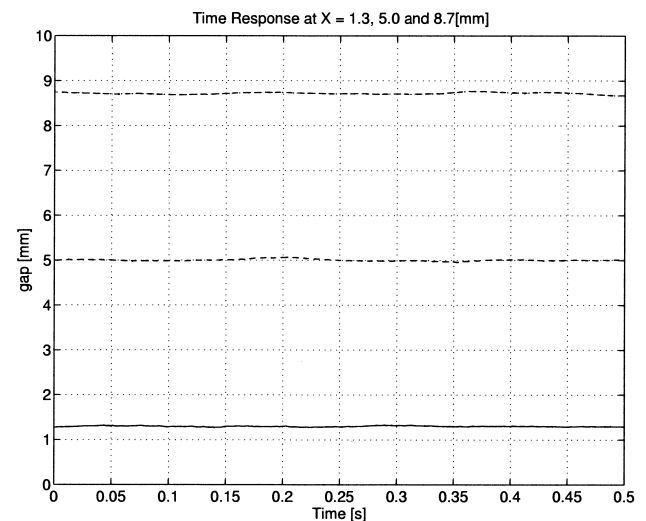


Fig. 12. Time Response at $X = 1.3, 5.0, 8.7$ mm

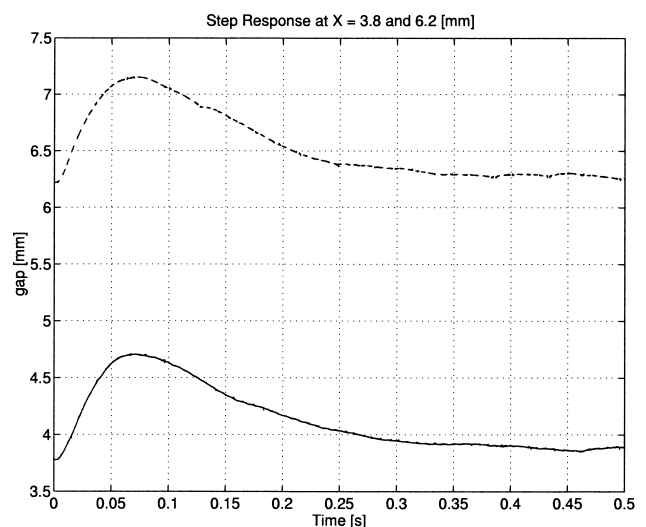


Fig. 13. Step Response at $X = 3.8, 6.2$ mm

7, 2000)

References

- (1) P. K. Sinha, *Electromagnetic Suspension: Dynamics and Control*, IEE, Peter Peregrinus, London, 1987.
- (2) G. Schweitzer, et al., *Active Magnetic Bearings*, Hochschulverlag AG an der ETH Zurich, 1994.
- (3) P.E. Allaire and D.L. Trumper (Editor): *Proceedings of the Sixth International Symposium on Magnetic Bearings*, Technomic Publishing Company, Inc., 1998.
- (4) Special Issue on Magnetic Bearings, *JSME International Journal Series C*, vol.40, no.4, pp.553-606, 1997.
- (5) C.R. Knospe and E.G. Collins (Editor): Special Issue on Magnetic Bearing Control, *IEEE Trans. on Control Systems Technology* vol.4, no.5, pp.481-608, 1996.
- (6) M. Fujita, T. Namerikawa, et al., " μ -Synthesis of an Electromagnetic Suspension System," *IEEE Trans. Automatic Control*, vol.40, no.3, pp.530-536, 1995.
- (7) F. Lösch, C. Gähler and R. Herzog, " μ -Synthesis Controller Design for a 3 MW Pump Running in AMBs," *Proc. of the Sixth Int. Symp. on Magnetic Bearings*, pp. 415-428, 1998.
- (8) K. Nonami and T. Ito: " μ Synthesis of a Flexible Rotor Magnetic Bearing Systems," *IEEE Trans. on Control Systems Technology*, vol.4, no.5, pp.503-512 1996.
- (9) T. Sugie and M. Kawanishi, "Analysis and Design of Magnetic Levitation Systems Considering Physical Parameter Perturbations," *Trans. of ISCTE*, vol.8, no.2, pp.70-79, 1995.
- (10) R. Fittro and C. Knospe, " μ Synthesis Control Design Applied to a High Speed Machining Spindle with Active Magnetic Bearings," *Proc. of the Sixth Int. Symp. on Magnetic Bearings*, pp.449-458, 1998.
- (11) M. Hirata, K. Nonami and T. Ohno, "Robust Control of a Magnetic Bearing System Using Constantly Scaled H_∞ Control," *Proc. of the Sixth Int. Symp. on Magnetic Bearings*, pp.713-722, 1998.
- (12) C. Beck, R. D'Andrea, F. Paganini and J.C. Doyle, "A State-Space Theory of Uncertain Systems," *Proc. of 13th IFAC World Congress*, pp.291-296, 1996.
- (13) P.M. Young, "Controller design with real parametric uncertainty," *Int. J. of Control*, vol.65, no.3, pp. 469-509, 1996.
- (14) F. Paganini, "Sets and Constraints in the Analysis of Uncertain Systems," *Ph.D. Thesis, California Institute of Technology*, 1996.
- (15) B.J.Balas, J.C.Doyle, K.Glover, A.Packard and R.Smith, *μ -Analysis and Synthesis Toolbox User's Guide*, MUSYN Inc. and Math Works, 1996.
- (16) K. Zhou and J.C. Doyle, *Essentials of Robust Control*, Prentice-Hall Int. Inc., 1998.

Masayuki Fujita (Member) He received the B.E., M.E. and Dr. of engineering degrees in electrical engineering from Waseda University, in 1982, 1984 and 1987, respectively. From 1995 until 1992, he was with Kanazawa University. From 1992 until 1998, he was with the Japan Advanced Institute of Science and Technology. In April 1998, he joined Kanazawa University, where he is presently a Professor in the Department of Electrical and Electronic Engineering. From 1994 to 1995, he held a visiting position in the Technical University of Munich, Germany. His research interests include robust control and its applications to robotics and mechatronics.



Toru Namerikawa (Member) He received the B.E., M.E. and Dr. of Engineering Degrees in electrical and computer engineering from Kanazawa University, Japan, in 1991, 1993 and 1997, respectively. Since 1994, he has been with Kanazawa University. He is currently an Assistant Professor in the Department of Electrical and Electronic Engineering. From 2001, he holds a visiting position in the University of California, Santa Barbara, USA. His research interests are robust control applications to electro-mechanical systems.

